Supplemental Material for Chaos-assisted long-range tunneling for quantum simulation

Maxime Martinez,[1] Olivier Giraud,[2] Denis Ullmo,[2] Juliette Billy,[3]
David Guéry-Odelin,[3] Bertrand Georgeot,[1] and Gabriel Lemarié[1,4,5]

[1] *Laboratoire de Physique Théorique, Université de Toulouse, CNRS, UPS, France*
[2] *Université Paris-Saclay, CNRS, LPTMS, 91405, Orsay, France*
[3] *Laboratoire Collisions Agrégats Réactivité, Université de Toulouse, CNRS, UPS, France*
[4] *MajuLab, CNRS-UCA-SU-NUS-NTU International Joint Research Unit, Singapore*
[5] *Centre for Quantum Technologies, National University of Singapore, Singapore*

In this Supplemental Material, we describe the methods used to numerically simulate the dynamical evolutions of the temporally modulated system and of the effective Hamiltonian, whose construction we explain in more details. The code we used is written in Python 3 and uses the Numpy library. It is available at https://framagit.org/mmartinez/dynamics1d. We then describe in detail the derivation of the hopping law. We also present a discussion on the relation between the classical transport in the chaotic sea and the quantum long range effect. We then give another simulation with a different set of parameters than the one in the main text showing that the effect is also visible in a more semiclassical (but still experimentally relevant) regime. We end with a discussion on the use of another quantity to characterize the spreading of the wave function.

Numerical methods

Exact dynamics of the periodically modulated lattice

The system, composed of N_c cells of spatial size $\lambda = 2\pi$ is discretized with N_p points per cell; the total basis size is thus $N_t = N_c N_p$. We have used both a spatial $|x\rangle$ and momentum $|p\rangle$ representation. The corresponding grids are centered around $x = 0$ and $p = 0$ with respective size-step:

$$\delta x = \frac{\lambda}{N_p} \quad \text{and} \quad \delta p = \frac{2\pi}{\lambda}\frac{\hbar_{\text{eff}}}{N_c}. \tag{1}$$

For the whole study, we took $N_p = 32$ after checking that this discretization was fine enough to faithfully represent the dynamics of the system: in particular, the total size in the p direction $N_p\hbar_{\text{eff}}$ should be larger than the extension of the chaotic sea in momentum space.

The time propagation of a given state $|\psi\rangle$ is achieved with a symmetrized split-step method:

$$|\psi(t+\delta t)\rangle = U_P F U_X F^{-1} U_P \,|\psi(t)\rangle\,, \tag{2}$$

with

$$U_X = \sum_x \exp\left(-i\frac{V(x,t)\delta t}{\hbar}\right)|x\rangle\langle x|\,,\; U_P = \sum_p \exp\left(-i\frac{p^2\delta t}{4\hbar}\right)|p\rangle\langle p| \tag{3}$$

$$F = \frac{1}{\sqrt{N}}\sum_{x,p}\exp\left(-i\frac{xp}{\hbar}\right)|p\rangle\langle x| \quad \text{(using FFT)}. \tag{4}$$

The time step $\delta t = 4\pi/1000$ was chosen after consistency tests.

Construction of the effective Hamiltonian

The determination of the Floquet-Bloch band is equivalent to the determination of the quasi-energy spectrum of the following Hamiltonian

$$H_\beta(x,t) = \frac{(p-\hbar_{\text{eff}}\beta)^2}{2} - \gamma(1+\varepsilon\cos t)\cos x, \tag{5}$$

on a single cell $N_c = 1$ (with $N_p = 32$, see above), with the quasi-momentum β taking the discrete values $\beta_m = 2\pi m/(N_c\lambda)$, $m = 0, \ldots, N_c - 1$. Thus, for a system size N_c, we repeat N_c times the following procedure (for each value of β_m):

- First, we build the matrix (in x reprentation) of the Floquet operator from the propagation of N_p δ-function states $|x\rangle$. To do so, we use the previous split-step method over two periods of modulation $T = 4\pi$ (this choice was made to be consistent with [1], but is of no importance here).
- Second, we diagonalize the Floquet operator and look for the eigenstate having the largest overlap with a Gaussian state centered on the regular island. This eigenstate is associated with a complex eigenvalue α_β that gives the effective energy:

$$\varepsilon_{\rm eff}^{\rm reg}(\beta) = -\frac{i\hbar_{\rm eff}}{T}\log\alpha_\beta. \tag{6}$$

- Once we have obtained the N_c values of $\varepsilon_{\rm eff}^{\rm reg}(\beta_m)$, we build explicitly the effective tight-binding Hamiltonian $H_{\rm eff}$, whose coupling elements $t_n^{\rm eff} \equiv \langle (m+n)_{\rm reg}|H_{\rm eff}|m_{\rm reg}\rangle$ are computed from the discrete Fourier Transform:

$$t_n^{\rm eff} = \frac{1}{N}\sum_{\beta_m} \varepsilon_{\rm eff}^{\rm reg}(\beta_m)\exp(i\beta_m\lambda n). \tag{7}$$

Dynamic evolution under the effective Hamiltonian

The effective Hamiltonian is a tight-binding model of N_c sites $|n\rangle$, with $n = 0, \ldots N_c - 1$. The wavefunction $|\psi\rangle$ is propagated over two periods with effective evolution propagator:

$$|\psi(t+T)\rangle = U_{\rm eff}\,|\psi(t)\rangle \quad \text{with} \quad U_{\rm eff} = \exp\left(-i\frac{H_{\rm eff}T}{\hbar_{\rm eff}}\right), \tag{8}$$

obtained using a Padé approximation.

Construction of the regular Wannier-states

The Wannier states of the unperturbed lattice (with $\varepsilon = 0$) provide an approximation of the regular modes $|n_{\rm reg}\rangle$ of the modulated lattice discussed in the letter. To construct them, we thus use a procedure similar to that used for the determination of the effective energy band, but using the unmodulated lattice (with $\varepsilon = 0$): For each value of $\beta_m = 2\pi m/(N_c\lambda)$, $m = 0, \ldots N_c - 1$, we diagonalize the evolution operator over two periods $T = 4\pi$ and look for the eigenstate having the largest overlap with a Gaussian state centered on the regular island. The p representation of this eigenstate gives the coefficient of the Wannier state on the partial (uncomplete) grid $p = \hbar_{\rm eff}\beta + n\delta p$ of size N_p. After repeating N_c times this procedure, we obtain the full p representation of the Wannier state (on the complete momentum basis of size N_pN_c).

Miscellaneous

The classical dynamics is simulated using a RK4 Runge-Kutta algorithm. Husimi phase-space representations are computed using the procedure described e.g. in [2].

Derivation of the hopping law for large system sizes

To derive the hopping law Eq. (3), we first decompose the effective Bloch band as a regular part ε_0 and a sum over all resonance terms:

$$\varepsilon_{\rm reg}^{\rm eff}(\beta) = \varepsilon_0(\beta) + \sum_{\rm resonances} \varepsilon_{\asymp}(\beta - \beta_0, W, \alpha), \tag{9}$$

where we assume that the evolution of the energy near each resonance is universal and only depends on three parameters: β_0 the position of the resonance, W the coupling intensity between the chaotic and the regular state and α the slope of the energy of the involved chaotic state with β. More precisely we consider that the system is locally described by a two-level Hamiltonian with an avoided crossing at $\beta' = \beta - \beta_0 = 0$:

$$\begin{pmatrix} \varepsilon_{\rm reg}(\beta') & W \\ W & \varepsilon_{\rm ch}(\beta') \end{pmatrix} \tag{10}$$

with $\varepsilon_{\rm reg}(\beta') = 0$ (since it is taken into account by ε_0 in Eq. (9)) and $\varepsilon_{\rm ch}(\beta') = \alpha\beta'$. The corresponding eigenstates $|\beta_\pm\rangle$ and eigenenergies $\varepsilon_\pm(\beta')$ follow:

$$\varepsilon_\pm(\beta') = \frac{\varepsilon_{\rm reg} + \varepsilon_{\rm ch}}{2} \pm \sqrt{\Delta^2 + W^2} \quad \text{and} \quad |\beta_\pm\rangle = \begin{cases} \cos\theta\,|\beta_{\rm reg}\rangle + \sin\theta\,|\beta_{\rm ch}\rangle \\ -\sin\theta\,|\beta_{\rm reg}\rangle + \cos\theta\,|\beta_{\rm ch}\rangle \end{cases}, \tag{11}$$

with $\Delta = (\varepsilon_{\rm reg} - \varepsilon_{\rm ch})/2$ and $\theta \in [0, \pi/2]$ verifying $\tan 2\theta = |W|/\Delta$. The prescription for the effective spectrum construction is to select the energy associated with the eigenstate having the largest projection on the regular subspace. We thus get:

$$\varepsilon_\asymp(\beta', W, \alpha) = \frac{\alpha}{2}\left(\beta' - \mathrm{sgn}(\beta')\sqrt{\beta'^2 + \left(\frac{2|W|}{\alpha}\right)^2}\right). \tag{12}$$

Taking the Fourier transform, we then have

$$t_n = t_n^0 + \sum_{\text{resonances}} t_n^\asymp(\beta_0, W, \alpha) \quad \text{with} \quad t_n^\asymp(\beta_0, W, \alpha) = \frac{\lambda}{2\pi}\int_{-\pi/\lambda}^{\pi/\lambda} \varepsilon_\asymp(\beta - \beta_0, W, \alpha) \mathrm{e}^{-in\beta\lambda}\,\mathrm{d}\beta\,. \tag{13}$$

We now assume that $\varepsilon_\asymp(\beta - \beta_0, W, \alpha)$ is peaked around β_0 and that β_0 is sufficiently far from the edge of the boundary of the Brillouin zone, so that

$$t_n^\asymp(\beta_0, W, \alpha) \approx \mathrm{e}^{in\beta_0\lambda}\frac{\lambda}{2\pi}\int_{-\pi/\lambda}^{\pi/\lambda} \varepsilon_\asymp(\beta, W, \alpha)\mathrm{e}^{-in\beta\lambda}\,\mathrm{d}\beta\,. \tag{14}$$

The latter expression can be evaluated for large n values. We introduce $x = \beta\lambda$ and $\eta = 2\lambda|W|/\alpha = \lambda\Delta\beta/2$, it reads

$$t_n^\asymp = \frac{\mathrm{e}^{in\beta_0\lambda}\alpha}{4\pi\lambda} \times \underbrace{\int_{-\pi}^{\pi}\left(x - \mathrm{sgn}(x)\sqrt{x^2+\eta^2}\right)\mathrm{e}^{-inx}\,\mathrm{d}x}_{I^*}, \tag{15}$$

we split the integral I (taking complex conjugation) in two parts, the first one gives

$$\int_{-\pi}^{\pi} x\mathrm{e}^{inx}\,\mathrm{d}x = \frac{2i\pi}{n}(-1)^{n+1}. \tag{16}$$

The second part can be rewritten

$$\int_0^{\pi} \mathrm{sgn}(x)\sqrt{x^2+\eta^2}\mathrm{e}^{inx}\,\mathrm{d}x - \text{c.c.}, \tag{17}$$

we then deform the contour of integration $0 \to \pi$ to a complex circuit $0 \to iT \to iT + \pi \to \pi$ with T some large real number. Using Watson's formula, the first part gives (setting $x = iy$)

$$i\int_0^T \sqrt{\eta^2 - y^2}\mathrm{e}^{-ny}\,\mathrm{d}y \sim \frac{i|\eta|}{n}. \tag{18}$$

The second part is negligible for T large enough (setting $x = y + iT$):

$$\mathrm{e}^{-nT}\int_0^{\pi} \sqrt{(y+iT)^2+\eta^2}\mathrm{e}^{-iny}\,\mathrm{d}y \to 0. \tag{19}$$

Using Watson's formula and assuming $\Delta\beta \ll \frac{2\pi}{\lambda}$ so that $(\eta/\lambda)^2 \ll 1$, the third part (setting $x = \pi + iy$) gives:

$$i(-1)^{n+1}\int_0^T \sqrt{(\pi+iy)^2+\eta^2}\mathrm{e}^{-ny}\,\mathrm{d}y \sim \frac{i\pi}{n}(-1)^{n+1}. \tag{20}$$

Putting all terms together (taking care of complex conjugation) we end up with

$$t_n^{\rightleftharpoons} \approx \frac{\mathrm{e}^{in\beta_0\lambda}\alpha}{4\pi\lambda}\left(\frac{2i\pi}{n}(-1)^{n+1} - \frac{2i\eta}{n} - \frac{2i\pi}{n}(-1)^{n+1}\right)^* = \frac{\mathrm{e}^{in\beta_0\lambda}\alpha}{4\pi\lambda} \times \frac{i4\lambda|W|}{|\alpha|} = \frac{i}{\pi n}\mathrm{sgn}(\alpha)|W|\mathrm{e}^{in\beta_0\lambda}. \tag{21}$$

We finally assume that t_n^0 is negligible for large n values (because it decays exponentially), so that

$$t_n \approx \frac{i}{\pi n}\sum_{\text{resonances}} \mathrm{sgn}(\alpha)|W|\mathrm{e}^{in\beta_0\lambda}. \tag{22}$$

Classical dynamics and quantum long-range properties

In the main text we discuss how the long-range chaos-assisted tunneling mechanism can be qualitatively inferred from a semiclassical picture. In the other hand, its appearance at quantum scale is a direct consequence of the existence of sharp and strong tunneling resonances in the band structure, which is a fairly generic feature of system whose classical dynamics is mixed. Hence it is not clear how the corresponding classical transport properties in the chaotic sea may affect this mechanism.

For instance, in the classical counterpart of the model we study, the motion in the chaotic sea is generically superdiffusive. Indeed, there exist large transporting islands (Fig. 1 of this Supplemental Material) centered around $p = \pm 1$ (which travel at constant speed $v = \lambda/T$) around which classical trajectories can stick for a long time, accelerating the usual diffusion process in the chaotic sea. As a consequence the value of the classical diffusion exponent depends a lot on the fine structure of the phase space, as is shown for three different sets of parameters in Fig. 1 of this Supplemental Material. However, this does not affect the quantum long range properties of the effective Hamiltonian, which remain essentially unchanged, see Fig. 2 of this Supplemental Material and Fig. 5 of the main text. Thus the quantum long range properties do not seem to depend on the details of the classical transport processes inside the chaotic sea.

Probing a deeper semiclassical regime ($\gamma = 0.15$, $\varepsilon = 0.60$ and $\hbar_{\text{eff}} = 0.2$)

We here present the comparison between the exact dynamics and the effective approach of a wavepacket initially located on a single regular site, for one of the sets of parameters presented in the previous section. The value of $\hbar_{\text{eff}} = 0.2$ was chosen smaller than in the main text ($\hbar_{\text{eff}} = 0.4$), to probe a more semiclassical regime (this value still remains relevant experimentally). The effective approach appears to be as good as in the other set of parameters (compare Figs. 3 and 4 of this Supplemental Material with Figs. 3 and 4 of the main text) and even better if one looks at the projection in the chaotic sea (Fig. 4b of this Supplemental Material) that saturates around $\sim 1.5\%$ to be compared with $\sim 5\%$ in the main text (Fig. 4b of the main text). This can be explained by the fact that in this regime the resonances are sharper. As an additional consequence of this smaller value of $\hbar_{\text{eff}}$, the unmodulated dynamics is totally frozen on the time scale we chose (Fig. 3), because the regular tunneling rate decreases exponentially with $\hbar_{\text{eff}}$.

Assessing the long range properties through the inverse participation ratio

In the main text we use the standard deviation of the spatial distribution of the wave packet to assess the long range properties of the system. Another popular quantity measuring the degree of localization of a wavefunction is the inverse participation ratio $\sum_n |\psi(n)|^4$. However, quite surprisingly, the participation ratio of a wavepacket initially located on a single regular site n_0 appears to poorly capture the long-range properties of the dynamics (Fig. 5 of this Supplemental Material). This can be explained if we note that the inverse participation ratio is dominated by the bulk of the distribution (the large wavefunction amplitudes), while long-range properties manifest themselves in long tails of the spatial probability distribution of the wavepacket. This also explains why the standard deviation of the

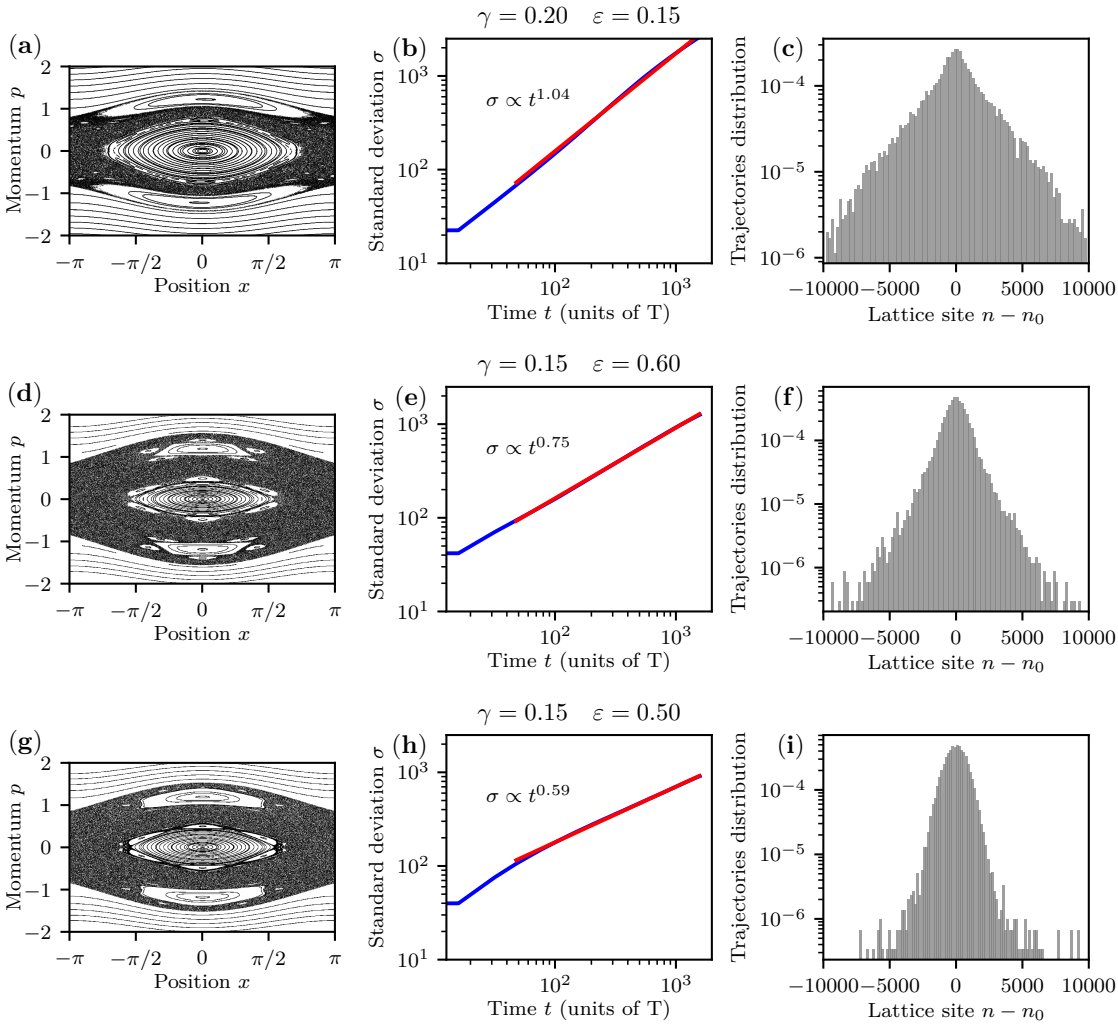

FIG. 1. Classical dynamics of Eq. (1) of the main text, for different set of parameters ((a-c) correspond to the parameters in the main text). (a,d,g) Stroboscopic phase portraits. (b,e,h) Standard deviation of the spatial distribution of a classical wavepacket initially launched in the chaotic sea (1799 trajectories launched around $(x_0, p_0) = (\pi, 0)$). Blue solid line for numerical data and red solid line for corresponding linear fit ($\log \sigma = a \log t + b$). The fitted value of the diffusion exponent a is given in the figure. (c,f,i) Corresponding spatial distribution at $t = 10000T$.

spatial distribution (which magnifies the long tails of the distribution) succeeds at revealing the long-range properties of the dynamics (see Fig 4 of the main text).

[1] M. Arnal, G. Chatelain, M. Martinez, N. Dupont, O. Giraud, D. Ullmo, B. Georgeot, G. Lemarié, J. Billy, and D. Guéry-Odelin, Science Advances **6**, eabc4886 (2020).
[2] M. Terraneo, B. Georgeot, and D. L. Shepelyansky, Phys. Rev. E **71**, 066215 (2005).

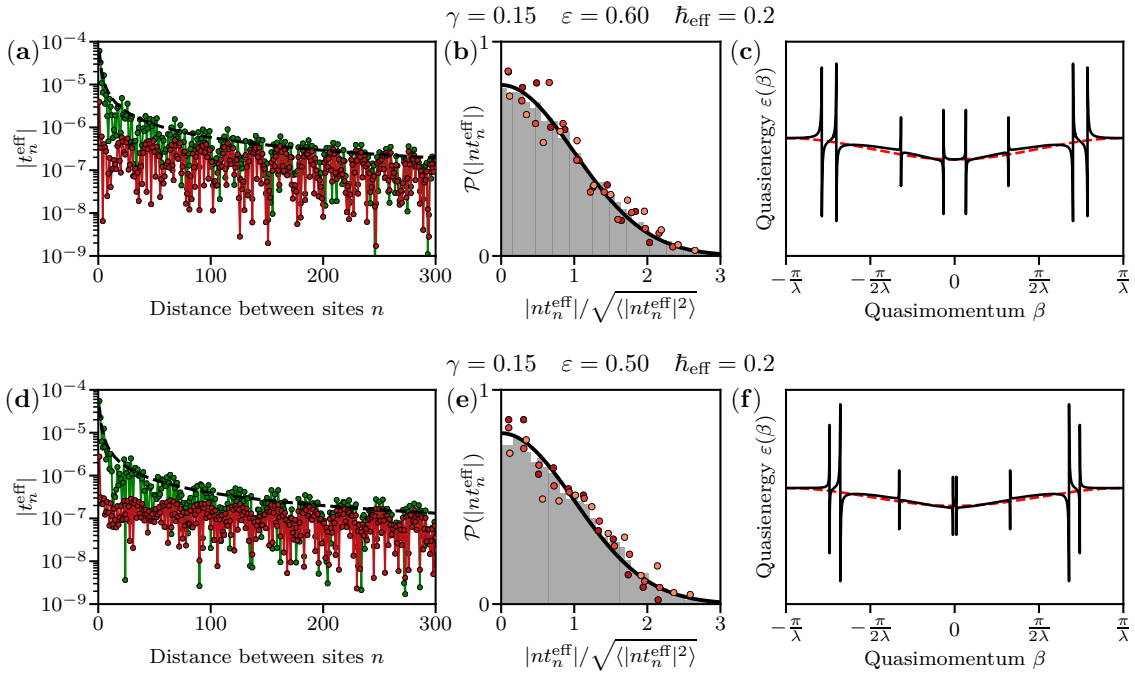

FIG. 2. (a,d) Effective hopping amplitude $|t_n^{\rm eff}|$ vs distance between sites n for different set of parameters. Red data were extracted from numerical Fourier series of the effective band structure. Green data correspond to Eq. 3 of the main text with parameters extracted from the band structure. Black solid line is the typical value of Eq. (3) of the main tex (without the phase term). (b,e) Distribution of fluctuations around the $1/n$ for the same parameters. Histogram corresponds to cumulative values for $1500 < n < 10000$, dots are partial datasets of 500 consecutive values of n, black curve is analytical prediction (see text). (c,f) Quasi-energy dispersion relation, black solid line is the effective regular band and red dashed line a nearest-neighbor approximation with parameters extracted from the effective regular band at $\beta = 0$ and $\beta = \pi/\lambda$.

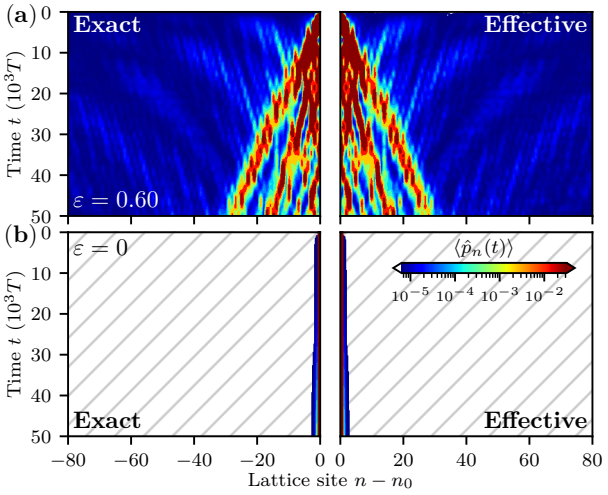

FIG. 3. Dynamics of a wavepacket, initially located on a single regular site n_0. Probability at each site vs time, with $\gamma = 0.15$, $\hbar_{\rm eff} = 0.2$ and $\varepsilon = 0.60$ for modulated lattice (a) or $\varepsilon = 0$ for unmodulated lattice (b). Exact dynamics (left) is compared with corresponding effective description (right), note that the system is symmetric through $n - n_0 \to n_0 - n$.

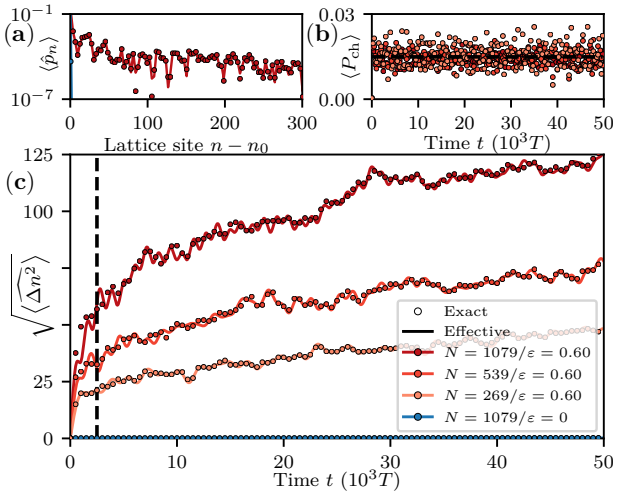

FIG. 4. Characterization of a wavepacket initially located on a single regular site n_0 (corresponding to Fig. 3 of this Supplemental Material). Symbols for exact dynamics and solid lines for effective dynamics. Red data for modulated lattices with different sizes, and blue data for unmodulated lattice. (a) Spatial probability distribution of the wavepacket after $t = 2500T$. (b) Overlap of the wavefunction with the chaotic sea vs time (see text). (c) Standard deviation of the spatial distribution vs time.

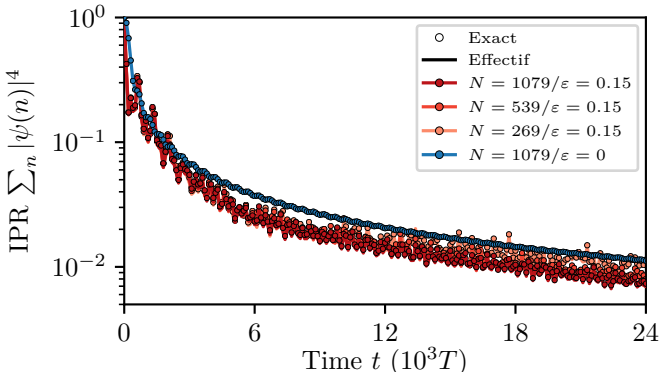

FIG. 5. Characterization of a wavepacket initially located on a single regular site n_0 (corresponding to Figs. 3 and 4 of the main text). The inverse participation ratio is plotted as a function of time. Symbols for exact dynamics and solid lines for effective dynamics. Red data for modulated lattices with different sizes, and blue data for unmodulated lattice.